



Parameter adjustments for optimizing signal integration using the FFT-DDI method

José Geraldo Telles Ribeiro¹ · Jaime Tupiassú Pinho de Castro² · Marco Antonio Meggiolaro²

Received: 19 January 2019 / Accepted: 13 January 2020
© The Brazilian Society of Mechanical Sciences and Engineering 2020

Abstract

Relative displacement measurements are needed in many practical applications, in particular to estimate damage from the associated strains and to follow and/or to control paths of moving objects. In many cases, such as monitoring of huge structures like tall bridges or of moving objects like vehicles, it is much easier to indirectly measure displacements by double-integrating an accelerometer signal, using some suitable numerical methods. However, such methods are susceptible to unknown initial conditions and to zero shifts, which may induce errors that are inadmissible in structural integrity evaluations and path control, so must be removed from the integrated signal. Many methods based on time-domain techniques are used in practice to decrease such zero-shifting errors; among them, the FFT-DDI method is used. Since this method is not well established yet, the purpose of this paper is to present some new techniques that can improve its efficiency.

Keywords Vibrating structures · Double integration · Accelerometers · Displacement

1 Introduction

Displacement measurements are often needed in many practical applications, for instance, to monitor machine movements, to calculate strain fields, or to follow and control paths of autonomous vehicles. Moreover, several works have used such measurements to study the dynamic behavior of bridges and civil structures [1, 2] and to evaluate the severity of earthquakes [3–5]. There are various kinds of non-inertial displacement gages available, based on capacitive, resistive, LVDT, eddy current, and optical sensors, but all such transducers need to be connected to some fixed reference close

to the point of measurement, since all of them are direct measurement devices. However, a close inertial reference may be very difficult to find in large structures, such as stadiums and bridges, and may be simply unavailable in the case of most moving objects. Indeed, when feasible, the construction of auxiliary inert structures like columns or rigid beams supported directly on rigid soil is expensive and time-consuming. GPS signals can be an option when the displacement resolution needed is in the order of meters, but in many practical cases, e.g., when the displacements should be used to calculate strains, such a resolution is simply not enough.

Moreover, since velocity and displacement seismic transducers cannot be made with both small size and low-frequency response, it is often necessary to indirectly measure displacements through the double integration of the signal generated by some appropriate acceleration transducer. Since there are commercial accelerometers with small size, good dynamic response, good reliability and affordable prices, they are a natural choice to measure structural vibrations. However, the precise measurement of displacements by integrating accelerometer signals is not a trivial task, as it might look at first sight. Indeed, even though there are many displacement-measuring devices available in the market that use analog circuits to double integrate accelerometer data, such integrators have no linear phase response for frequencies typically below 10 Hz; thus, these circuits

Technical Editor: Wallace Moreira Bessa, D.Sc..

✉ José Geraldo Telles Ribeiro
jose.ribeiro@uerj.br

Jaime Tupiassú Pinho de Castro
jtcastro@puc-rio.br

Marco Antonio Meggiolaro
meggi@puc-rio.br

¹ Department of Mechanical Engineering, State University of Rio de Janeiro - UERJ, Rio de Janeiro, RJ, Brazil

² Department of Mechanical Engineering, Pontifical Catholic University of Rio de Janeiro - PUC-Rio, Rio de Janeiro, RJ, Brazil

can much distort transient signals. Hence, this method may not be accurate and/or reliable enough for most practical applications [6].

Digital integration techniques, such as the trapezoidal rule or the Simpson 1/3 rule, can solve most of those problems, since they do not introduce errors due to nonlinear phase response. In principle, a digital integration scheme can be easily implemented by using the sampled signal measured by a data acquisition system. However, digital integration has its own problems, since it is very sensitive to the signal low-frequency components, which introduce a time-increasing error in the displacement signals. Since the integration has a cumulative characteristic, these errors cause drift or a zero-shifting type error, a problem that is magnified when the signal is double-integrated. Such errors are simply inadmissible for structural integrity evaluation purposes, because they would be associated with false strains and stresses of increasing magnitude. Direct GPS-based displacement measurements are another option, but as mentioned above the resolution obtainable from these devices is still not enough for measuring the small displacements needed in most structural integrity evaluations, even though they can be reduced using data fusion [7–12].

Therefore, since accelerometers still are the best choice for most dynamic measurements, many recent works are available in the literature proposing methods for decreasing the errors of the double integration of accelerations data, without using data fusion [13–21]. However, most of these methods are based on time-domain techniques that use least squares data-fitting methods and digital filters, which induce distortions of the signal as a side effect of the digital filtering [13, 14].

On the other hand, the FFT-DDI method [22–26] removes the zero shift of the signal in the frequency domain, avoiding time aliasing induced by digital filtering in the time domain [24]. The FFT-DDI is not a recent proposal, but it presents good results and has the advantage of not distorting the signal. However, its parameters (such as acquisition time, sample rate and number of samples) that optimize its application are not well established yet. Hence, the purpose of this paper is to present the most recent advances of the FFT-DDI method that can be used to establish the correct parameters to acquire acceleration signals.

2 Sources of errors in the digital integration

Without loss of generality, the extended trapezoidal rule is used throughout this paper. This method obeys Eq. (1), where $v^T(k)$ is the estimation for the actual value of the velocity $v(t)$ at t_k :

$$v^T(k) = v_0 + \frac{\Delta t}{2} \sum_{l=1}^k [a(l-1) + a(l)] \quad k = 1, \dots, N-1. \quad (1)$$

To calculate the approximate displacements, this same equation must be used once again on the calculated velocity. Equation (2) is the estimation of the displacement $x(t)$ at the instant t_k :

$$x^T(k) = x_0 + \frac{\Delta t}{2} \sum_{l=1}^k [v^T(l-1) + v^T(l)] \quad k = 1, \dots, N-1. \quad (2)$$

Incorrect estimates of the initial conditions are a source of error in Eqs. (1) and (2). Another source of error is the zero shift, a constant value superimposed on the actual acceleration signal $a(t)$ as shown in Eq. (3). This error is present in any real transducer output:

$$a_m(k) = a(k) + d \quad k = 0, 1, \dots, N-1. \quad (3)$$

Hence, the actual initial velocity and zero shift must be correctly estimated to obtain the correct velocity signal. Incorrect estimates of any of these variables result in an incorrect estimated velocity as shown in Eq. (4), where v_i and d_e are the estimations of the initial velocity and of the zero shift:

$$v^e(k) = v^T(k) + (v_0 - v_i) + (d - d_e) \cdot k \cdot \Delta t \quad k = 0, 1, \dots, N-1. \quad (4)$$

Finally, if the actual displacement x_0 is not known and is assumed incorrectly as x_i , the displacement will be estimated incorrectly as shown in Eq. (5):

$$x^e(k) = x^T(k) + (x_0 - x_i) + (v_0 - v_i) \cdot k \cdot \Delta t + \frac{d - d_e}{2} \cdot (k\Delta t)^2 \quad k = 0, \dots, N-1. \quad (5)$$

3 Time-domain trend removal

Equations (3), (4) and (5) show that an incorrect estimation of the initial velocity and displacement is equivalent to introduce a zero drift in them. Hence, only the acceleration estimate needs to be studied, since the same method to remove zero shift can be applied in each integration stage. A common way to estimate and remove such errors is to use the least squares method to calculate the mean value of the acceleration, the resulting linear velocity signal and the quadratic curve of the double-integrated displacement. This method, named time-domain trend removal (TDTR), is presented next. If the acceleration has a zero-mean value, a common method used to remove the zero-shift error is to calculate the mean value of the measured acceleration:

$$d_e = \frac{1}{N} \sum_{k=0}^{N-1} a^m(k) = \frac{1}{N} \sum_{k=0}^{N-1} [a(k) + d] = d + \frac{1}{N} \sum_{k=0}^{N-1} a(k). \quad (6)$$

The estimated zero shift will then be equal to the actual zero shift if and only if

$$\frac{1}{N} \sum_{k=0}^{N-1} a(k) = 0. \quad (7)$$

However, this is not always true. Suppose the acceleration is a sinusoidal signal defined by

$$a(k) = \sin\left(2\pi f_1 k \frac{T}{N} + \phi\right) \quad k = 0, 1, \dots, N - 1. \quad (8)$$

Then, the estimated mean value using the acquired data becomes

$$\begin{aligned} \frac{1}{N} \sum_{k=0}^{N-1} \sin\left(2\pi f_1 k \frac{T}{N} + \phi\right) \\ = \frac{\cos(\phi)[1 - \cos(2\pi f_1 T)] + \sin(\phi) \sin(2\pi f_1 T)}{2\pi f_1 T}. \end{aligned} \quad (9)$$

Equation (9) shows that this mean value is zero for any ϕ if $f_1 T$ is an integer. Otherwise, the mean value depends on ϕ . Suppose now that the acceleration is a damped sinusoidal signal defined by

$$a(k) = e^{-\sigma k \frac{T}{N}} \cdot \sin\left(2\pi f_1 k \frac{T}{N}\right) \quad k = 0, 1, \dots, N - 1. \quad (10)$$

Then, the estimated mean value using the acquired data becomes

$$\begin{aligned} \frac{1}{N} \sum_{k=0}^{N-1} e^{-\sigma k \frac{T}{N}} \cdot \sin\left(2\pi f_1 k \frac{T}{N}\right) \\ = \frac{1}{T} \frac{2\pi f_1 - e^{-\sigma N \Delta t} [\sigma \sin(2\pi f_1 T) - 2\pi f_1 \cos(2\pi f_1 T)]}{\sigma^2 + (2\pi f_1)^2}. \end{aligned} \quad (11)$$

Equation (11) shows that this mean value is not be zero for any ϕ , even if $f_1 T$ is an integer. Hence, there are situations when Eq. (6) does not estimate correctly the zero shift, resulting in a parabolic term in the estimated displacement as shown in Eq. (5). This explains the necessity of using least squares methods to remove this trend in displacement signals.

4 The FFT-DDI method

This section presents the fundamentals the FFT-DDI method. First, consider the FFT of a sampled discrete function, defined as

$$G(n) = \sum_{k=0}^{N-1} g(k) e^{-j2\pi \frac{n}{N} k} \quad n = 0, 1, \dots, N - 1 \quad (12)$$

where the FFT $G(n)$ is defined at the frequencies

$$f = \frac{n}{T} \quad n = 0, 1, \dots, \frac{N}{2} \quad (13)$$

It is important to review some characteristics of the FFT of some common functions to understand the method.

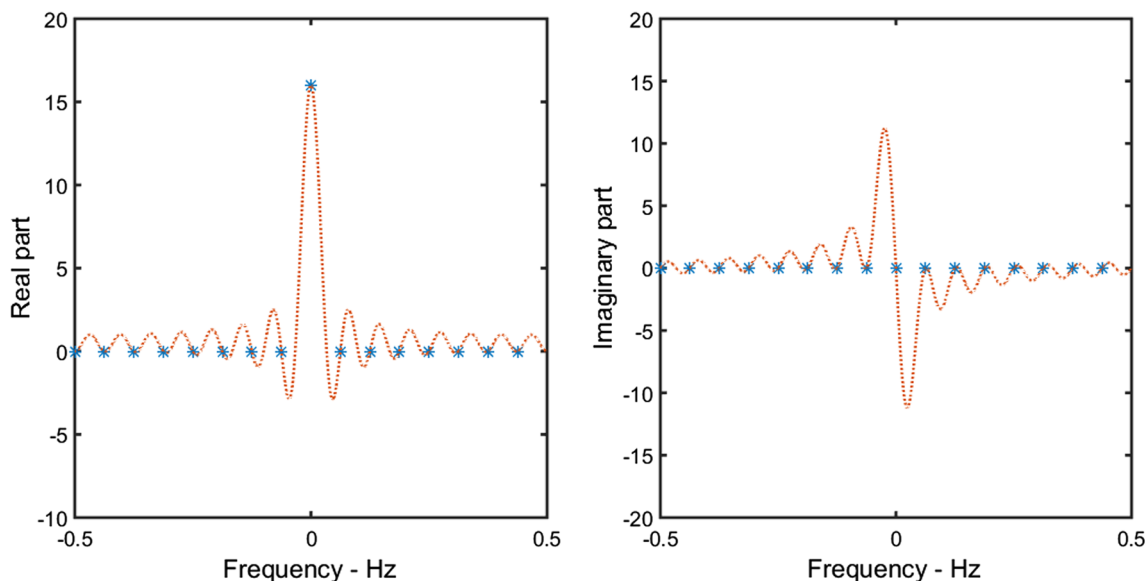


Fig. 1 Typical FFT of the unit step function with 16 sampled points

Figure 1 is the FFT of the unit step function defined by Eq. (14), with $T = N = 16$:

$$g(k) = 1 \quad k = 0, 1, \dots, N - 1 \tag{14}$$

$$G(n) = \begin{cases} N & \text{if } n = 0 \\ 0 & \text{elsewhere} \end{cases} \tag{15}$$

Figure 2 is the FFT of a sinusoidal function with $f_1 T$ not an integer, defined by

$$g(k) = \sin\left(2\pi \frac{4.7}{16} k\right) \quad k = 0, 1, \dots, N - 1. \tag{16}$$

Figure 3 is the FFT of a damped sinusoidal function with $f_1 T$ being an integer, defined by

$$g(k) = e^{-0.1k} \cdot \sin\left(2\pi \frac{4}{16} k\right) \quad k = 0, 1, \dots, N - 1. \tag{17}$$

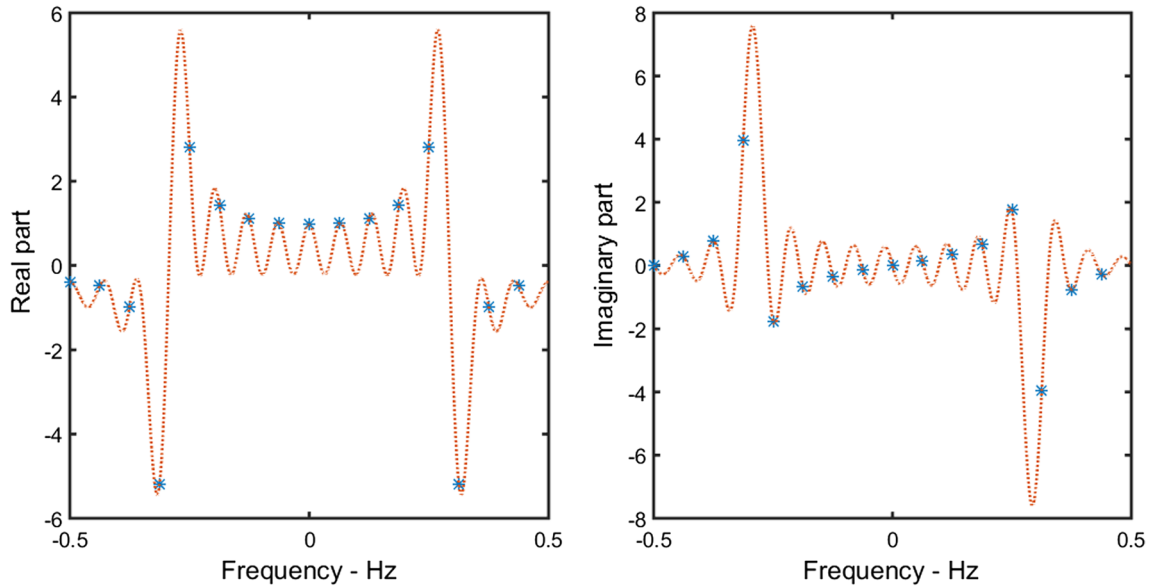


Fig. 2 Typical FFT of a sinusoidal function with 16 points sampled when $f_1 T$ is not an integer

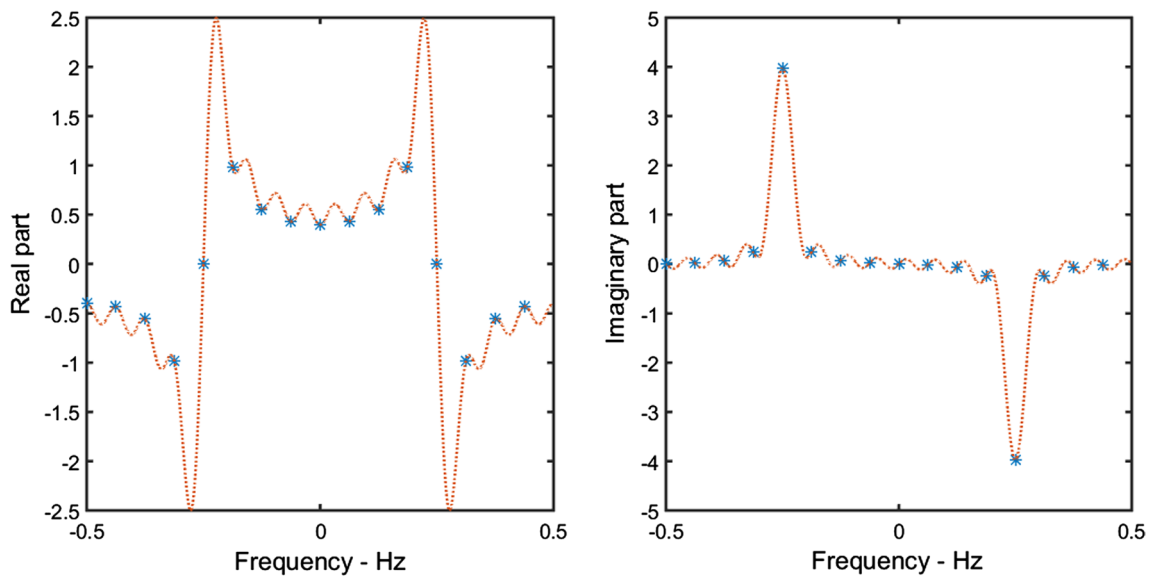


Fig. 3 Typical FFT of a damped sinusoidal function with 16 points sampled

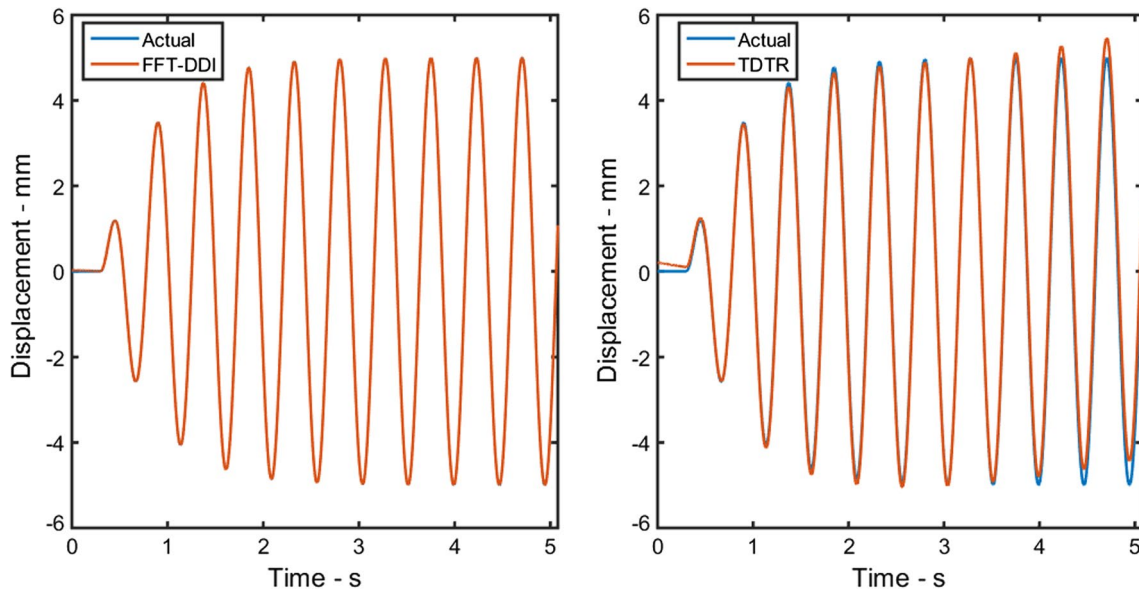


Fig. 4 Double integration of the acceleration associated with the displacements of Eq. (26), with the vibration starting at $t_1 = 0.30$ s

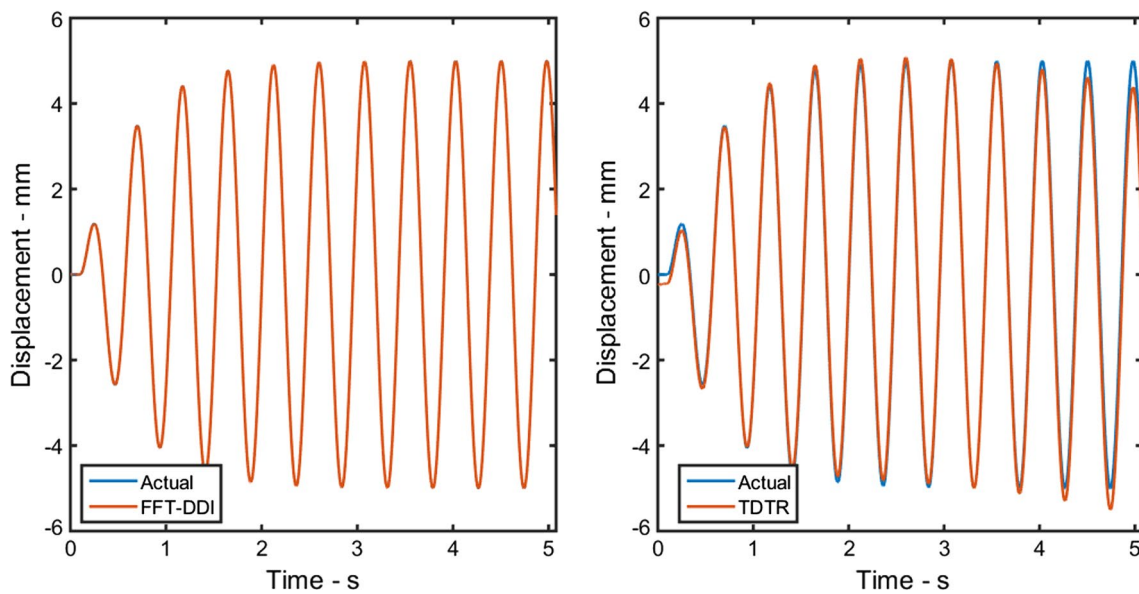


Fig. 5 Double integration of the acceleration associated with the displacements of Eq. (26), with the vibration starting at $t_1 = 0.10$ s

The FFT $G(n)$ of any function has one characteristic that will be the base of the FFT-DDI method: the value of $G(0)$ is proportional to the mean value of $g(k)$, as shown in Eq. (18).

$$G(0) = \sum_{k=0}^{N-1} g(k) = N \cdot \hat{\mu}_g \quad n = 0, 1, \dots, N - 1. \quad (18)$$

From Figs. 1, 2 and 3, it can be verified that:

Table 1 Summary of Fig. 4 results

Parameter	Actual	FFT-DDI		TDTR	
		Calculated	Error %	Calculated	Error %
Peak-to-valley	+10.0	+10.00	0.00	+10.50	5.00
Peak	+5.00	+5.00	0.00	+5.46	9.20
Valley	-5.00	-5.00	0.00	-5.04	0.80%

Table 2 Summary of Fig. 2 results

Parameter	Actual	FFT-DDI		TDTR	
		Calculated	Error %	Calculated	Error %
Peak-to-valley	+10.0	+10.00	0.00	+10.58	5.8
Peak	+5.00	+5.00	0.00	+5.08	1.6
Valley	-5.00	-5.00	0.00	-5.50	10

- the only influence of a constant value on the FFT of the acceleration is at $n = 0$;

- for any real valued function, the imaginary part at $n = 0$ is zero; and
- the real part of the FFT is an even function.

The solution proposed by the FFT-DDI method is then to estimate the value of the FFT of the signal at $n = 0$ using the values of the vicinity, but a good estimator has not been established yet.

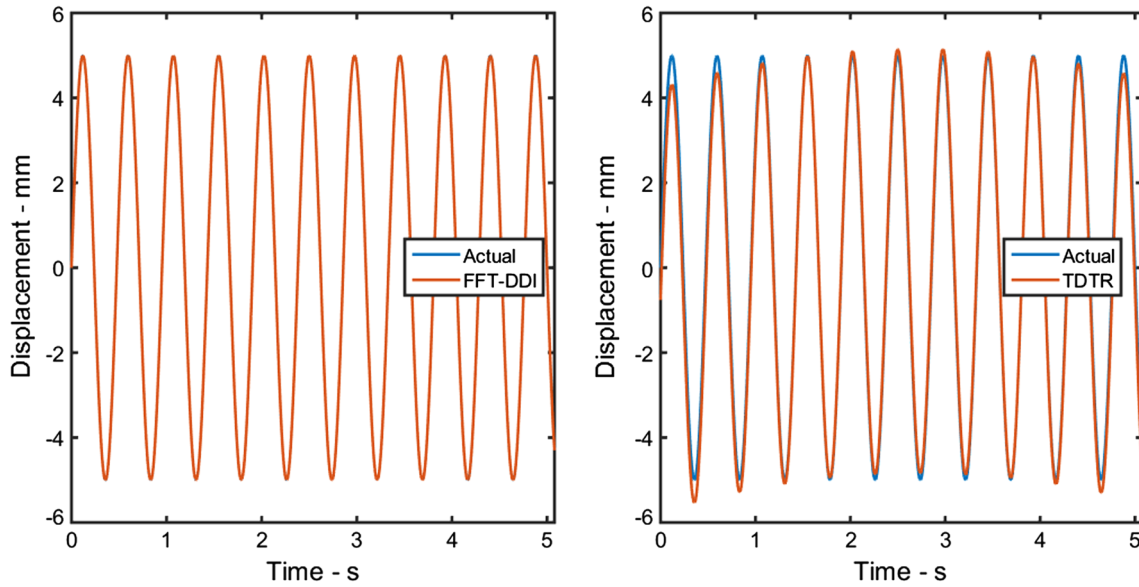


Fig. 6 Double integration of the acceleration associated with the displacement of Eq. (27), with $\phi = 0$ rad

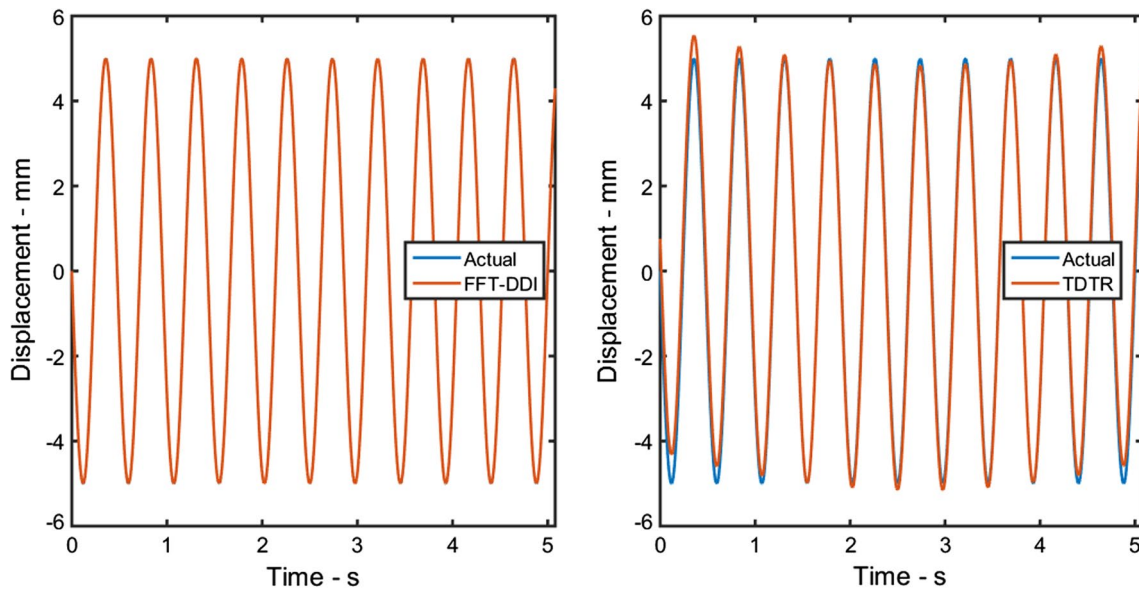


Fig. 7 Double integration of the acceleration associated with the displacement of Eq. (27), with $\phi = 0$ rad

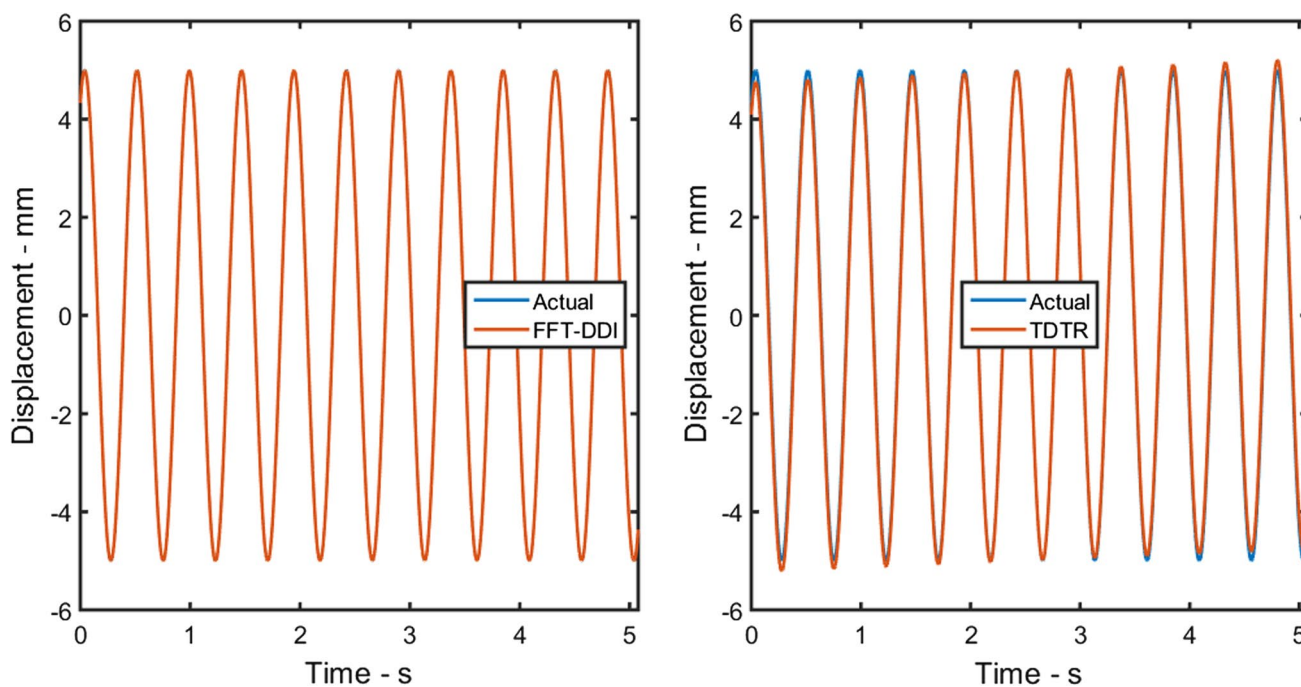


Fig. 8 Double integration of the acceleration associated with the displacement of Eq. (27), with $\phi = \pi/3$ rad

Table 3 Summary of Fig. 6 results

Parameter	Actual	FFT-DDI		TDTR	
		Calculated	Error %	Calculated	Error %
Peak-to-valley	+10.0	+10.00	0.00	+10.67	6.70
Peak	+5.00	+5.00	0.00	+5.15	3.00
Valley	-5.00	-5.00	0.00	-5.54	10.80

Table 4 Summary of Fig. 7 results

Parameter	Actual	FFT-DDI		TDTR	
		Calculated	Error %	Calculated	Error %
Peak-to-valley	+10.0	+10.00	0.00	+10.67	6.70
Peak	+5.00	+5.00	0.00	+5.54	10.80
Valley	-5.00	-5.00	0.00	-5.15	3.00

Table 5 Summary of Fig. 8 results

Parameter	Actual	FFT-DDI		TDTR	
		Calculated	Error %	Calculated	Error %
Peak-to-valley	+10.0	+10.00	0.00	+10.41	4.10
Peak	+5.00	+5.00	0.00	+5.20	4.00
Valley	-5.00	-5.00	0.00	-5.22	4.40

5 Parameter adjustment for the FFT-DDI method

Some other characteristics of the FFT of the harmonic signals must be verified to establish a better estimator:

- if the fundamental frequency of the signal is sufficiently high, the real part of the FFT at low frequencies can be approximated by a polynomial function.
- From Figs. 2 and 3, it can be deduced that this fundamental frequency component f_{min} must be equal or higher than $5/T$.
- Since these low-frequency components are not affected by the zero shift, this polynomial can be used to estimate the value $G(0)$ by interpolation.

Using these assumptions, it can be established that the minimum acquisition time must be obtained using Eq. (19):

$$T_{min} = \frac{5}{f_{min}} \tag{19}$$

Using this acquisition time, the low-frequency components at n from 1 to 3 can be used to obtain the polynomial. Furthermore, due to the symmetry of the real part of the FFT of a real function, it can be obtained by a polynomial of fifth order, as shown in Eq. (20):

$$p(n) = b_5n^5 + b_4n^4 + b_3n^3 + b_2n^2 + b_1n + b_0 \tag{20}$$

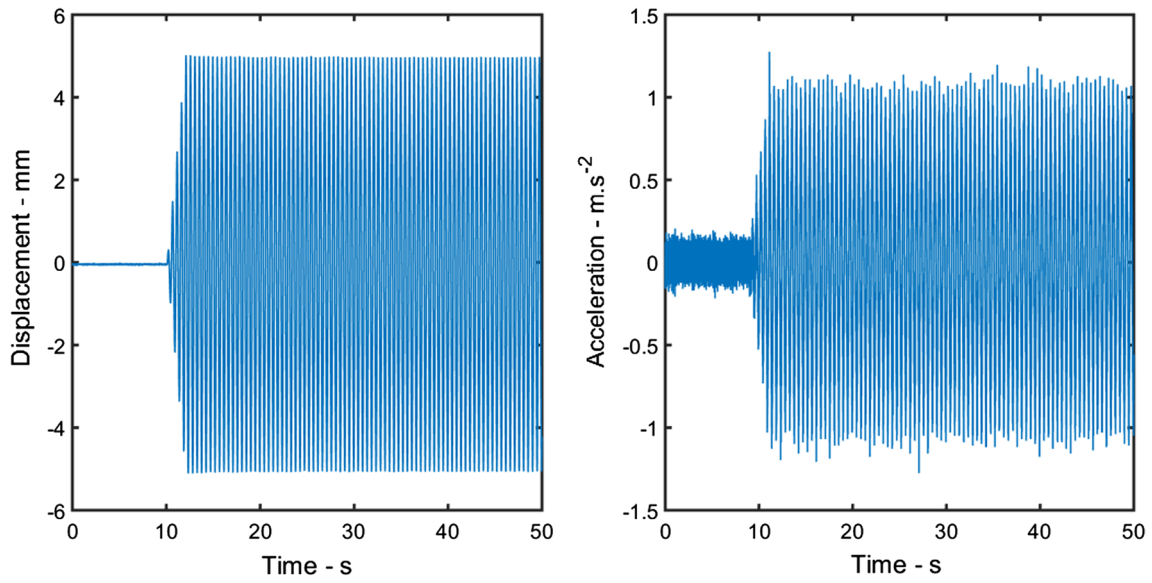


Fig. 9 Measurements of the displacements and accelerations

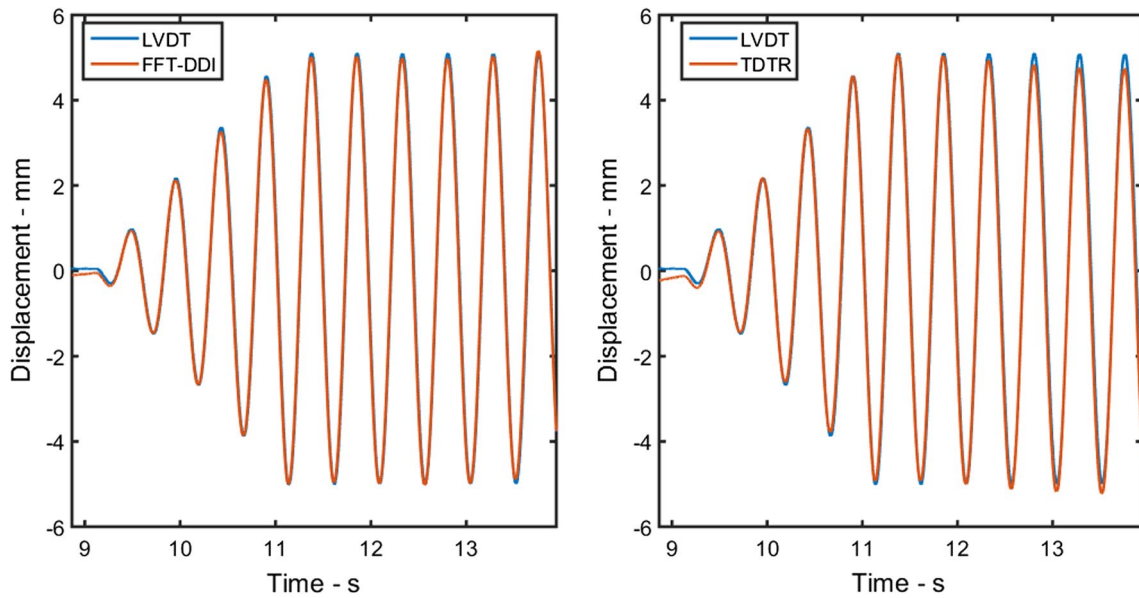


Fig. 10 Double integration of 8192 points of the acceleration of Fig. 9, from $t_1 = 8.87$ s

The constants of the polynomial can be obtained solving the linear system shown in Eq. (21), where $A^m(n)$ is the FFT of the measured acceleration and $A_r^m(n)$ is its real part:

$$\begin{bmatrix} (-3)^5 & (-3)^4 & (-3)^3 & (-3)^2 & (-3)^1 & 1 \\ (-2)^5 & (-2)^4 & (-2)^3 & (-2)^2 & (-2)^1 & 1 \\ (-1)^5 & (-1)^4 & (-1)^3 & (-1)^2 & (-1)^1 & 1 \\ 3^5 & 3^4 & 3^3 & 3^2 & 3^1 & 1 \\ 2^5 & 2^4 & 2^3 & 2^2 & 2^1 & 1 \\ 1 & 1 & 1 & 1 & 1 & 1 \end{bmatrix} \begin{bmatrix} b_5 \\ b_4 \\ b_3 \\ b_2 \\ b_1 \\ b_0 \end{bmatrix} = \begin{bmatrix} p(-3) \\ p(-2) \\ p(-1) \\ p(1) \\ p(2) \\ p(3) \end{bmatrix} = \begin{bmatrix} A_r^m(3) \\ A_r^m(2) \\ A_r^m(1) \\ A_r^m(1) \\ A_r^m(2) \\ A_r^m(3) \end{bmatrix} \quad (21)$$

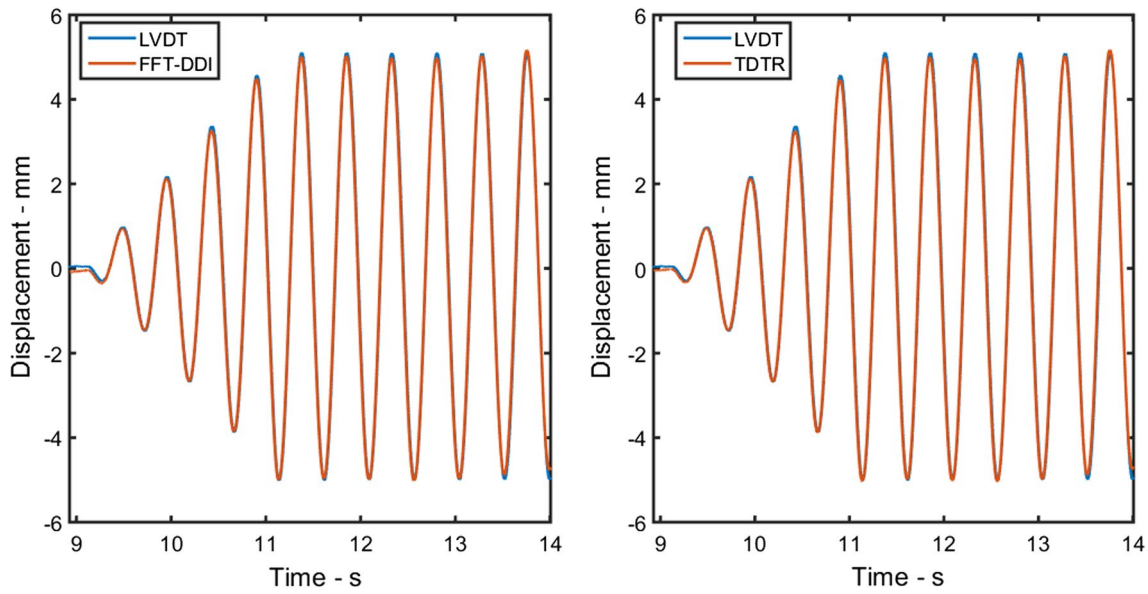


Fig. 11 Double integration of 8192 points of the acceleration of Fig. 9, from $t_1 = 8.93$ s

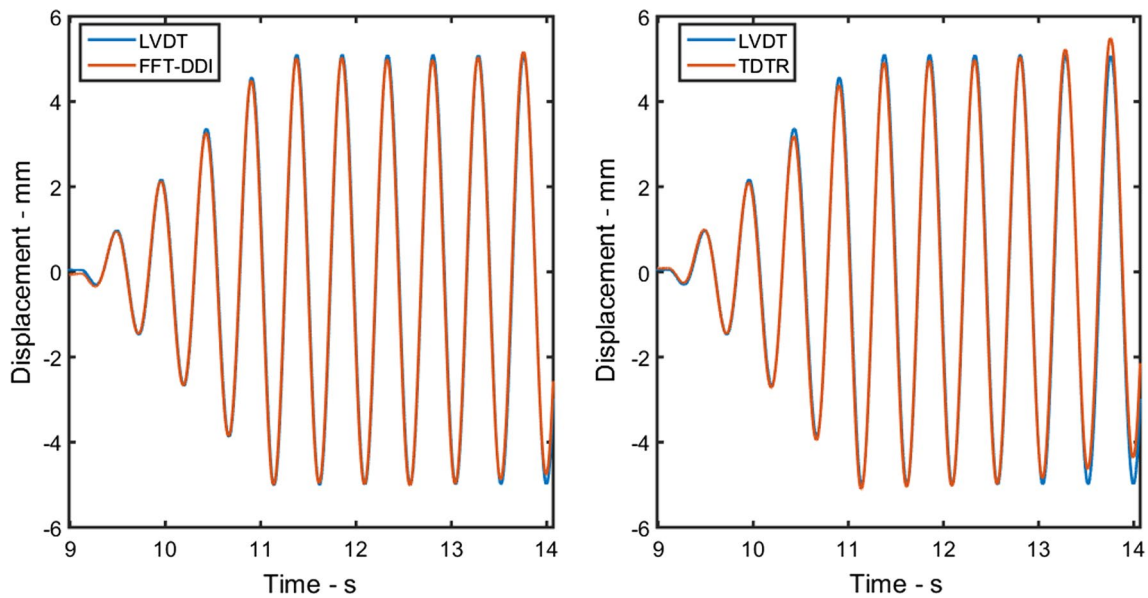


Fig. 12 Double integration of 8192 points of the acceleration of Fig. 9, from $t_1 = 8.99$ s

The objective of this polynomial is to obtain the value of the FFT of the actual acceleration at $n = 0$. Then, it is necessary to calculate b_0 only, as shown in Eq. (22):

$$p(0) = b_0 \cong A(0). \tag{22}$$

Using Cramer's rule, b_0 can be calculated using

$$b_0 = \frac{\begin{vmatrix} (-3)^5 & (-3)^4 & (-3)^3 & (-3)^2 & (-3)^1 & A_r^m(3) \\ (-2)^5 & (-2)^4 & (-2)^3 & (-2)^2 & (-2)^1 & A_r^m(2) \\ (-1)^5 & (-1)^4 & (-1)^3 & (-1)^2 & (-1)^1 & A_r^m(1) \\ 3^5 & 3^4 & 3^3 & 3^2 & 3^1 & A_r^m(3) \\ 2^5 & 2^4 & 2^3 & 2^2 & 2^1 & A_r^m(2) \\ 1 & 1 & 1 & 1 & 1 & A_r^m(1) \end{vmatrix}}{691200} \tag{23}$$

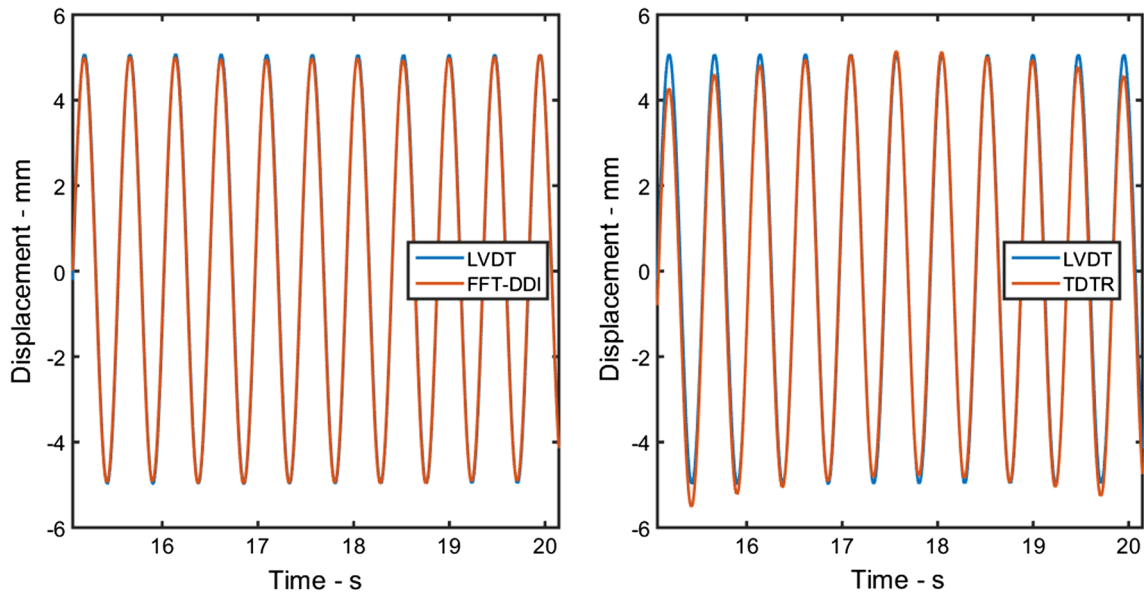


Fig. 13 Double integration of 8192 points of the acceleration of Fig. 9, from $t_1 = 15.07$ s

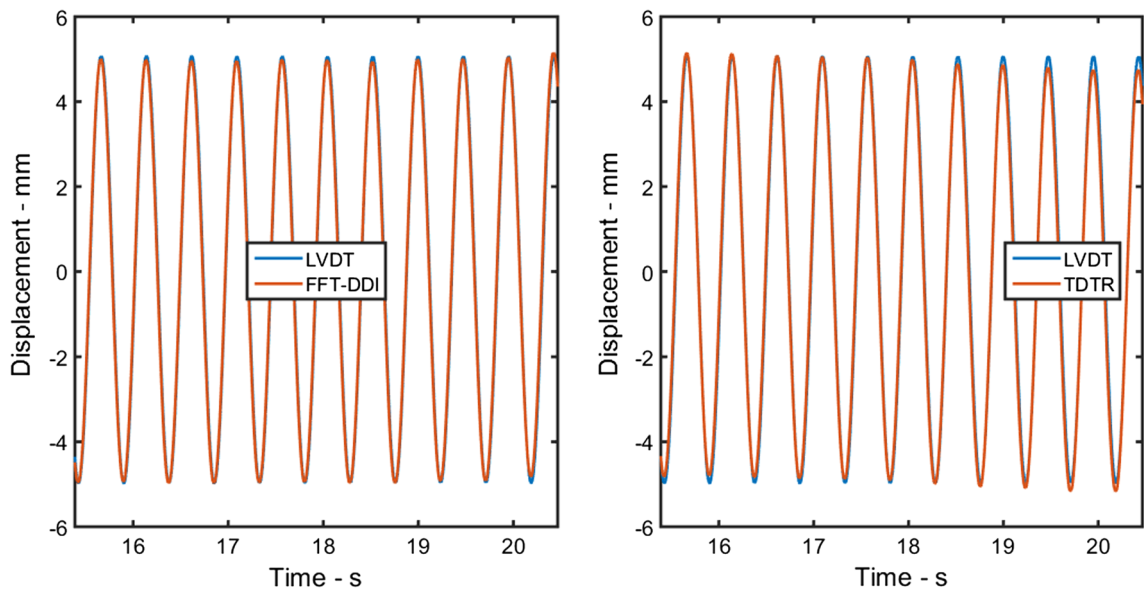


Fig. 14 Double integration of 8192 points of the acceleration of Fig. 9, from $t_1 = 15.39$ s

The zero shift of the acceleration can be estimated using Eq. (24):

$$d \approx \frac{A^m(0) - b_0}{N} \tag{24}$$

If the condition of Eq. (19) is valid, this estimation will be much better than the estimation obtained using Eq. (6). Then, the actual acceleration can be calculated using Eq. (25):

$$a(k) = a^m(k) - \frac{A^m(0) - b_0}{N} \quad k = 0, 1, \dots, N - 1. \tag{25}$$

This acceleration can be used to obtain the velocity using Eq. (1), considering $v_i = 0$. If this estimation is incorrect, it will introduce a zero shift in velocity that is equal the actual initial velocity, as shown in Eq. (4). Then, the same process can be used to remove this zero shift and to obtain the velocity that will be used to obtain the displacement using Eq. (2).

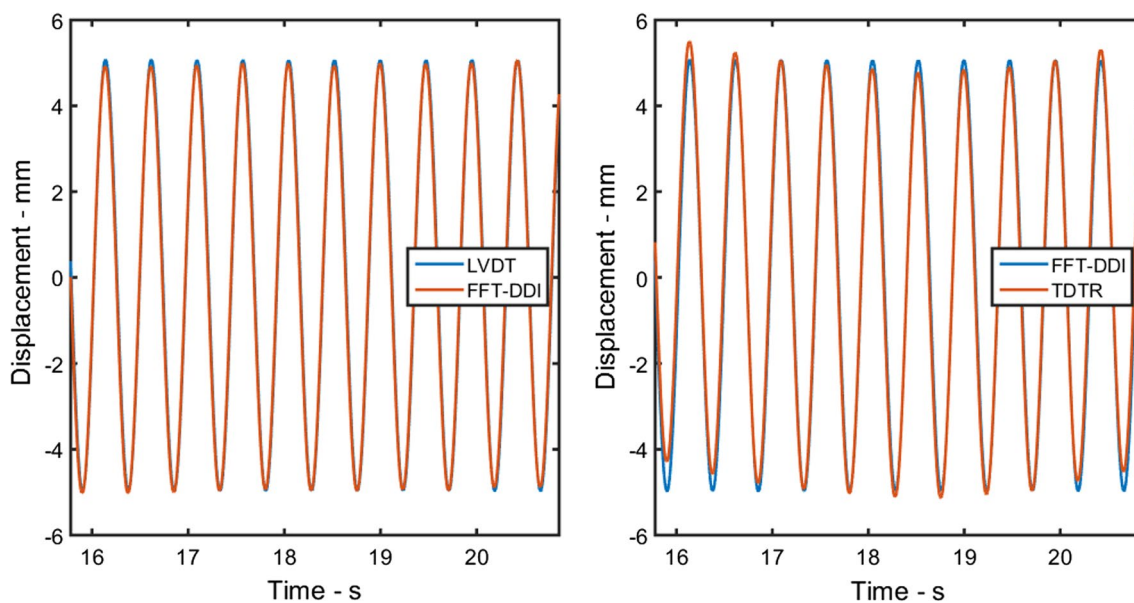


Fig. 15 Double integration of 8192 points of the acceleration of Fig. 9, from $t_1 = 15.78$ s

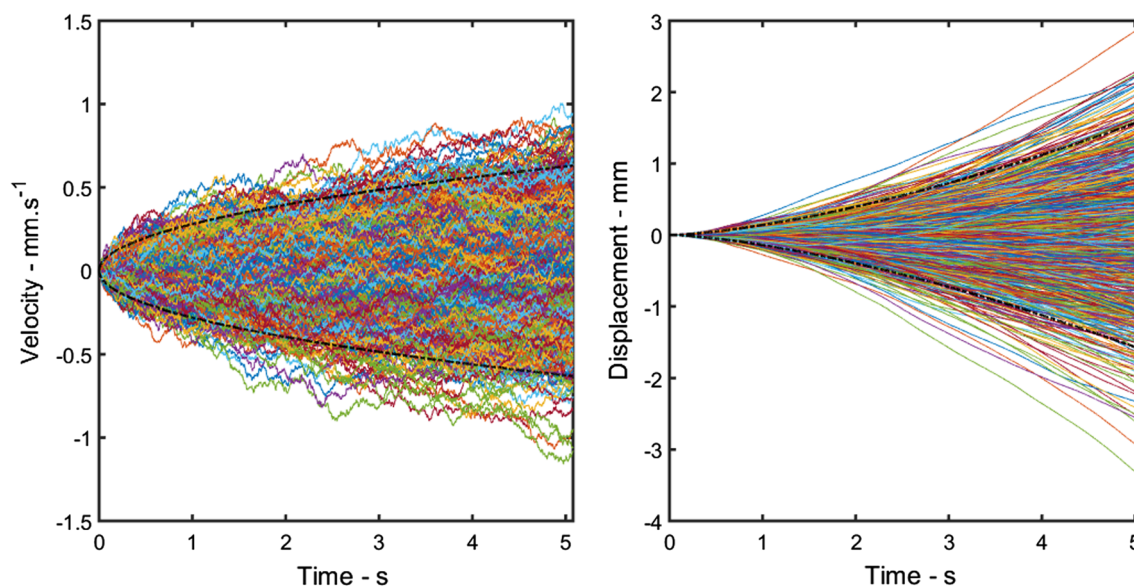


Fig. 16 Velocities and displacements obtained using the trapezoidal rule on white noise signals

Table 6 Summary of Fig. 10 results

Parameter	Actual	FFT-DDI		TDTR	
		Calculated	Error (%)	Calculated	Error (%)
Peak-to-valley	10.13	10.17	0.39	10.30	1.68
Peak	5.11	5.15	0.78	5.08	-0.58
Valley	-5.02	-5.02	0.00	-5.22	3.98

Table 7 Summary of Fig. 11 results

Parameter	Actual	FFT-DDI		TDTR	
		Calculated	Error %	Calculated	Error %
Peak-to-valley	10.13	10.18	0.49	10.21	0.79
Peak	5.11	5.16	0.98	5.17	1.17
Valley	-5.02	-5.02	0.00	-5.04	0.39

Table 8 Summary of Fig. 12 results

Parameter	Actual	FFT-DDI		TDTR	
		Calculated	Error %	Calculated	Error %
Peak-to-valley	10.13	10.19	0.59	10.59	4.54
Peak	5.11	5.17	1.17	5.49	7.44
Valley	-5.02	-5.02	0.00	-5.10	1.59

Table 9 Summary of Fig. 13 results

Parameter	Actual	FFT-DDI		TDTR	
		Calculated	Error %	Calculated	Error %
Peak-to-valley	10.09	10.05	-0.40	10.66	5.65
Peak	5.09	5.07	-0.39	5.15	1.18
Valley	-5.00	-4.98	-0.40	-5.51	10.20

Table 10 Summary of Fig. 14 results

Parameter	Actual	FFT-DDI		TDTR	
		Calculated	Error %	Calculated	Error %
Peak-to-valley	10.09	10.13	0.40	10.32	2.28
Peak	5.09	5.15	1.17	5.15	1.17
Valley	-5.00	-5.00	0.00	-5.17	3.40

Table 11 Summary of Fig. 15 results

Parameter	Actual	FFT-DDI		TDTR	
		Calculated	Error %	Calculated	Error %
Peak-to-valley	10.09	10.09	0.00	10.64	5.45
Peak	5.09	5.07	-0.39	5.50	8.06
Valley	-5.00	-5.02	0.40	-5.13	2.60

6 Numerical simulations

In the simulations below, it is supposed that a structure at a stationary position starts vibrating from instant t_1 and that this vibration is monitored with an acceleration measurement system that acquires $N = 8192$ points with a sample time interval $\Delta t = 0.00062$ s, leading to an acquisition time of $T = 5$ s. The displacement during this period is expressed by

$$x(t) = -X \cdot \left[1 - e^{-\sigma(t-t_1)} \right] \cdot \sin \left[2\pi \cdot f_1 \cdot (t - t_1) \right] \quad t \geq t_1. \tag{26}$$

Consider that the structure vibrates with an amplitude $X = 5$ mm, at a frequency $f_1 = 2.1$ Hz, and that $\sigma = 2$. The results of the double integration of the measured acceleration

are shown in Figs. 4 and 5, and the results are summarized in Tables 1 and 2.

After the transient, the displacement is expressed by

$$x(t) = -X \cdot \sin \left(2\pi \cdot f_1 \cdot t + \phi \right). \tag{27}$$

The value of the phase angle ϕ depends on the initial value of the acceleration. The results of the double integration of the acceleration are shown in Figs. 6, 7 and 8, and the results are summarized in Tables 3, 4 and 5.

7 Experimental validation

The experimental validation is performed generating a sinusoidal displacement signal with 5 mm amplitudes at the frequency of 2.1 Hz using an Instron 8501 servo-hydraulic machine equipped with an LVDT, which was used as the reference displacement transducer.

The acceleration is measured using a resistive accelerometer model AS-1G from Kyowa Electronic Instruments, connected to a signal conditioner model NI 9237 from National Instruments. The acquisition system is connected to a desktop using Windows 10 and LabVIEW 2014. The acquisition sampling time has been set as $\Delta t = 0.00062$ s. Figure 9 shows the acceleration signal measured using the accelerometer, as well as the displacement signal measured using the LVDT. The results of both studied methods are shown in Fig. 10, 11, 12, 13, 14, 15 and 16, with the results summarized in Tables 6, 7, 8, 9, 10 and 11.

8 Effects of the noise

Noise is any undesirable spurious signal that contaminates measurements reducing their resolution and accuracy. Hence, noise can be another important error source in practical measurements. In accelerometers, noise is generated by their electrical and mechanical components, as well as by their amplifier and cables [25]. Assuming noise can be modeled as a Gaussian wide band, it can be characterized by its statistical parameters, its mean and variance. The mean value of the noise can be estimated from

$$\hat{\mu}_a = \frac{1}{N} \sum_{i=1}^N a_i, \tag{28}$$

while the variance of the noise can be estimated using

$$\hat{\sigma}_a^2 = \frac{1}{N} \sum_{i=1}^N (a_i - \mu_a)^2. \tag{29}$$

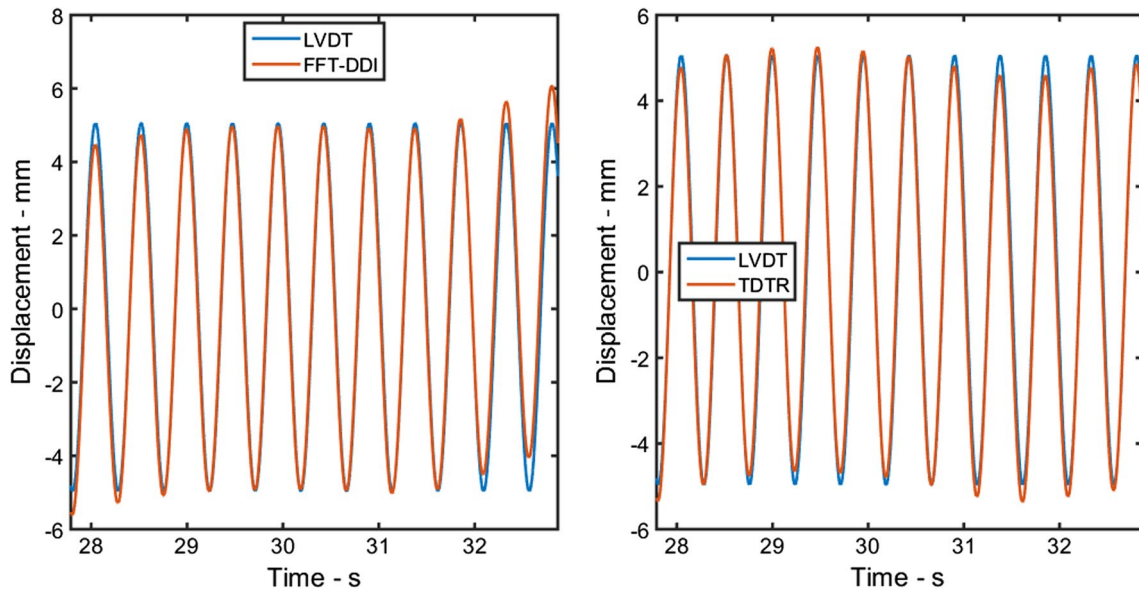


Fig. 17 Double integration of 8192 points of the acceleration of Fig. 9, from $t_1 = 27.79$ s

Table 12 Summary of Fig. 17 results

Parameter	Actual	FFT-DDI		TDTR	
		Calculated	Error %	Calculated	Error %
Peak-to-valley	10.06	11.69	16.20	10.62	5.57
Peak	5.08	6.07	19.50	5.25	3.35
Valley	-4.98	-5.61	12.65	-5.36	7.63

Table 13 Summary of Fig. 18 results

Parameter	Actual	FFT-DDI		TDTR	
		Calculated	Error %	Calculated	Error %
Peak-to-valley	10.06	10.05	0.01	10.39	3.28
Peak	5.08	5.04	-0.79	5.09	0.20
Valley	-4.98	-5.01	0.60	-5.30	6.43

Since the noise is a random process, its mean value has a Gaussian distribution centered at zero and the variance of its estimation can be estimated using

$$\text{Var}[\hat{\mu}_a] \approx \frac{\sigma_a^2}{2BT}. \tag{30}$$

In Eq. (30), B is the bandwidth of the signal and T is acquisition time. The random error of the estimate $\hat{\mu}_a$ has a standard deviation:

$$\sigma[\hat{\mu}_a] \approx \frac{1}{\sqrt{2T}} \frac{\sigma_a}{\sqrt{B}}. \tag{31}$$

Therefore, there is a probability of about 95% that the estimate $\hat{\mu}_a$ falls within the interval [26]:

$$[-2 \cdot \sigma[\hat{\mu}_a] \leq \hat{\mu}_a < 2 \cdot \sigma[\hat{\mu}_a]]. \tag{32}$$

Considering an initial velocity $v_0 = 0$ in the integration of the noise, the velocity at sample k can be estimated using

$$v^T(k) \approx \hat{\mu}_{a_k} \cdot k\Delta t. \tag{33}$$

Using Eq. (32), it can be deduced that the probability the estimate $v^T(k)$ will fall within the interval:

$$[-2k\Delta t \cdot \sigma[\hat{\mu}_{a_k}] \leq v^T(k) < 2k \cdot t\Delta\sigma[\hat{\mu}_{a_k}]] \tag{34}$$

is about 95%. Using Eq. (31), then

$$\left[-2k\Delta t \frac{1}{\sqrt{2k\Delta t}} \frac{\sigma_a}{\sqrt{B}} \leq v^T(k) < 2k\Delta t \frac{1}{\sqrt{2k\Delta t}} \frac{\sigma_a}{\sqrt{B}} \right] \tag{35}$$

which becomes

$$\left[-\sqrt{2} \cdot \frac{\sigma_a}{\sqrt{B}} \cdot t^{1/2} \leq v^T(k) < \sqrt{2} \cdot \frac{\sigma_a}{\sqrt{B}} \cdot t^{1/2} \right]. \tag{36}$$

Considering an initial displacement $x_0 = 0$ in the integration of v^T , the displacement at sample k can be estimated using

$$x^T(k) \approx \frac{1}{2} \hat{\mu}_{a_k} (k\Delta t)^2. \tag{37}$$

Using a similar method, it can be deduced that the probability that the estimate $x^T(k)$ will fall within the interval

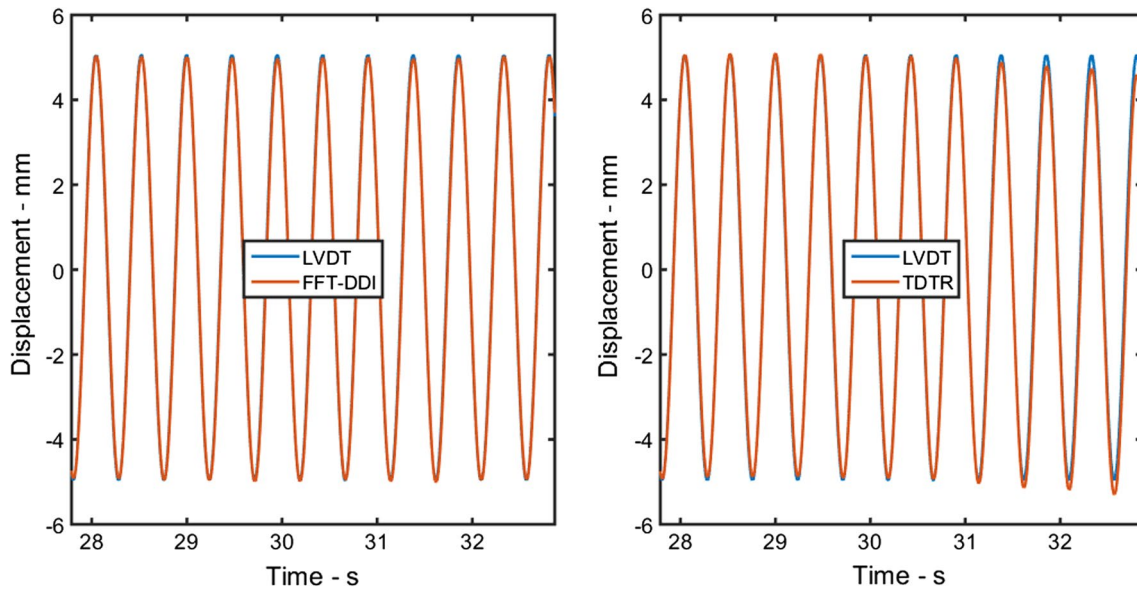


Fig. 18 Double integration of 8192 points of the acceleration of Fig. 9 after filtered using a high-pass FIR filter, from $t_1 = 27.79$ s

$$\left[-\frac{\sqrt{2}}{2} \cdot \frac{\sigma_a}{\sqrt{B}} \cdot t^{3/2} \leq x^T(k) < \frac{\sqrt{2}}{2} \cdot \frac{\sigma_a}{\sqrt{B}} \cdot t^{3/2} \right] \quad (38)$$

is about 95%.

Figure 16 shows the integration and double integration results using the trapezoidal rule of several noise signals with standard deviation $\sigma_a = 5.62 \text{ mm s}^{-2}$, using $N = 8192$ points with a sample time of $\Delta t = 0.00062$ s, leading to an acquisition time period $T = 5$ s. The confidence interval shown in Eq. (36) for velocity and Eq. (38) for displacement is represented in the dotted lines of the figures.

Figure 17 shows the double integration of a sample of the acceleration shown in Fig. 9, with a huge error that was not present in the previous results. This error is due to the noise present in the measurement system, which has a standard deviation $\sigma_a = 5.62 \text{ mm s}^{-2}$ (Tables 12 and 13).

Then, the acceleration signal is filtered using a high-pass FIR filter with a cutoff frequency of 0.7 Hz and used to obtain the displacement using both methods. The results are shown in Fig. 18.

9 Conclusions

The FFT-DDI showed good results in past works [24, 25], but the methodology of removing the zero shift was not well established, so the method was not easy to use. The parameter fitting procedure proposed in Sect. 5 can be used to minimize displacement errors introduced in double numerical integrations of an acceleration data. The first important piece of information in the proposed methodology is the

fundamental frequency of the acceleration. Using this information, the minimum time acquisition is calculated using Eq. (19). The sample rate and the number of samples do not affect the zero shift removal; thus, they must be chosen based on the error of the integration method used. The removal of the zero shift of the acceleration can be done by calculating its FFT and using in sequence Eqs. (23), (24) and (25). The removal of the zero shift of the calculated velocity and displacement can be done in a similar process. The simulations and experimental validation showed that this method presented results much better than the baseline correction using least squares methods. Finally, it must be emphasized that noise is a huge source of error. It corrupts the displacement signal in both methods. But after a convenient filtering of the signal, the FFT-DDI presented the best results.

References

1. Fenerci A, Øiseth O, Rønnquist A (2017) Long-term monitoring of wind field characteristics and dynamic response of a long-span suspension bridge in complex terrain. *Eng Struct* 147:269–284
2. Sekiya H, Maruyama O, Miki C (2017) Visualization system for bridge deformations under live load based on multipoint simultaneous measurements of displacement and rotational response using MEMS sensors. *Eng Struct* 146:43–53
3. Guorui HU, Tao LU (2015) Review on baseline correction of strong-motion accelerogram. *Int J Sci Technol Soc* 3(6):309–314
4. Heng L, Jianchao W, Yunsheng Y, Xiaojun Q (2012) Baseline correction for near-fault ground motion recordings of the 2008 Wenchuan Ms8.0 earthquake. *Geodesy Geodyn* 3(2):60–70

5. Heng L, Yunsheng Y, Shuiming Z, Yongjian C, Dongning L (2011) Baseline correction for digital strong-motion records by using the pre-event portion. *Geodesy Geodyn* 2(1):43–46
6. Ribeiro JGT; Castro JTP, Freire JLF (1997) Problems in analogue double integration to determine displacements from acceleration data. In: *Proceedings of the 15th international modal analysis conference, Orlando, Florida*. pp 930–934
7. Xu Y, Brownjohn JMW, Hester D, Koo KY (2017) Long-span bridges: enhanced data fusion of GPS displacement and deck accelerations. *Eng Struct* 147:639–651
8. Zheng Z et al (2019) Data fusion based multi-rate Kalman filtering with unknown input for on-line estimation of dynamic displacements. *Measurement* 131:211–218
9. Kim K et al (2018) Structural displacement estimation through multi-rate fusion of accelerometer and RTK-GPS displacement and velocity measurements. *Measurement* 130:223–235
10. Han H, Wang J, Meng X, Liu H (2016) Analysis of the dynamic response of a long span bridge using GPS/accelerometer/anemometer under typhoon loading. *Eng Struct* 122:238–250
11. Moschas F, Stiros S (2011) Measurement of the dynamic displacements and of the modal frequencies of a short-span pedestrian bridge using GPS and an accelerometer. *Eng Struct* 33(1):10–17
12. Kim J, Kim K, Sohn H (2014) Autonomous dynamic displacement estimation from data fusion of acceleration and intermittent displacement measurements. *Mech Syst Signal Process* 42(1–2):194–205
13. Zheng W et al (2019) Real-time dynamic displacement monitoring with double integration of acceleration based on recursive least squares method. *Measurement* 141:460–471
14. Arias-Lara D, De-La-Colina J (2018) Assessment of methodologies to estimate displacements from measured acceleration records. *Measurement* 114:261–273
15. Lu Y-S, Wang H-W, Liu S-H (2018) An integrated accelerometer for dynamic motion systems. *Measurement* 125:471–475
16. Hester D, Brownjohn J, Bocian M, Xu Y (2017) Low cost bridge load test: Calculating bridge displacement from acceleration for load assessment calculations. *Eng Struct* 143:358–374
17. Lotfi B, Huang L (2016) An approach for velocity and position estimation through acceleration measurements. *Measurement* 90:242–249
18. Abir J et al (2016) Optimized estimator for real-time dynamic displacement measurement using accelerometers. *Mechatronics* 39:1–11
19. Pan J, Zhang C, Zhang X (2016) Real-time accurate odometer velocity estimation aided by accelerometers. *Measurement* 91:468–473
20. Hong YH, Lee SG, Lee HS (2013) Design of the FEM-FIR filter for displacement reconstruction using accelerations and displacements measured at different sampling rates. *Mech Syst Signal Process* 38(2):460–481
21. Hong YH, Kim HK, Lee HS (2010) Reconstruction of dynamic displacement and velocity from measured accelerations using the variational statement of an inverse problem. *J Sound Vib* 329(23):4980–5003
22. Ribeiro JGT, Castro JTP, Freire JLF (1999) Some comments on digital integration to measure displacements using accelerometers. In: *Proceedings of the 17th international modal analysis conference, Kissimmee, Florida, vol 3727(2)*, pp 554–559
23. Ribeiro JGT, Castro JTP, Freire JL (2001) New improvements in the digital double integration filtering method to measure displacements using accelerometers. In: *Proceedings of the 19th international modal analysis conference, Orlando, Florida*, pp 538–542
24. Ribeiro JGT, Castro JTP, Freire JL (2002) Filtering in frequency domain to avoid time aliasing. In: *Proceedings of the 20th international modal analysis conference, Los Angeles, California*
25. Ribeiro JGT, Castro JTP, Freire JL (2003) Using the FFT-DDI method to measure displacements with piezoelectric, resistive and ICP accelerometers. In: *Proceedings of the 21st international modal analysis conference, Orlando, Florida*
26. Bendat JS, Piersol AG (2011) *Random data: analysis and measurement procedures*. Wiley, Hoboken

Publisher's Note Springer Nature remains neutral with regard to jurisdictional claims in published maps and institutional affiliations.